than by the excursion in either one of these activity indices considered alone.

The magnitude of the 4- to 9-month variations in total solar irradiance discussed here is consistent with the observed photometric contrast in visible light of spots and large faculae, and with their measured area variation (*13*). The simplest and best studied model of photospheric faculae explains their excess brightness as a direct result of their intense, vertical magnetic fields (*6*). Assuming even approximate magnetohydrostatic equilibrium, these kilogauss fields must reduce the local plasma pressure and thus its opacity. According to this model, this enables radiation to escape from deeper and hotter photospheric layers. The same effect should operate in spots, but in these larger diameter flux tubes, the inhibition of convective heat transport to the surface is expected to more than compensate, thus perhaps explaining their darkness.

The slower trends in total irradiance that we attribute to the decay of the network faculae may be explainable in terms of the same model of faculae as local heat leaks, although estimates of the facular network contrast and slow variations in area are difficult. The photometric contrast of faculae is known to increase roughly as inverse wavelength λ^{-1} (*14*) and is relatively large in the ultraviolet continuum (*15*). Estimates of the total irradiance variation expected from facular radiations of wavelength below 300 nm (*16*) suggest that a significant fraction of the total irradiance variations might arise from changing outputs from these magnetic structures in the 200- to 300-nm spectral region.

It is clearly of interest to test our model with a longer time base of radiometry. The variations studied here have amplitudes that are at the limit of the long-term calibration stability of either the ACRIM or ERB considered alone. It is highly desirable that the operation of both radiometers be maintained at least through the peak of the next solar cycle expected around 1991. Such measurements should finally resolve the classical question of the amplitude and phase of the total solar irradiance variability over the activity cycle, and begin the investigation of possible longer term secular trends in total solar output, such as those suggested by recent photometric analysis of sun-like main sequence stars (*17*).

REFERENCES AND NOTES

1. An early investigation of activity cycle influences on the solar constant was presented by C. Abbot, F. Fowle, and L. Aldrich [*Ann. Smithsonian Astrophys. Obs.* **3**, 129 (1913)].
2. Some recent discussions of this topic are: J. Eddy, R. Gilliland, D. Hoyt, *Nature* **300**, 689 (1982); G. Reid, *ibid.* **329**, 142 (1987); K. Labitzke, *Geophys. Res. Lett.* **14**, 535 (1987).
3. The ERB and ACRIM radiometers on the Nimbus-7 and SMM satellites, respectively, are discussed by J. Hickey *et al.* [*Science* **208**, 281 (1980)] and by R. Willson [*Appl. Opt.* **18**, 179 (1979)].
4. P. Foukal and J. Lean, *Astrophys. J.* **328**, 347 (1988).
5. R. C. Willson, S. Gulkis, M. Janssen, H. S. Hudson, G. A. Chapman, *Science* **211**, 700 (1981).
6. The photometric contrast of faculae has been measured by many investigators; see, for example, R. Muller, *Solar Phys.* **45**, 105 (1975); H. Wang and H. Zirin, *ibid.* **110**, 281 (1987). The cause of excess facular brightness has been investigated through physical models by a number of authors; see, for example, H. Spruit, *Solar Phys.* **50**, 269 (1976); S. Walton, *Astrophys. J.* **312**, 909 (1987); W. Deinzer *et al.*, *Astron. Astrophys.* **139**, 435 (1984). Other ideas have been put forward by K. Schatten, H. Mayr, and K. Omidvar [*J. Geophys. Res.* **92**, 818 (1987)].
7. The mechanisms of microwave emission from the chromospheric and coronal plage overlying photospheric faculae have been well discussed recently by K. Tapping [*J. Geophys. Res.* **92**, 795 (1987)]. The correlation of microwave emission variations at 10.7 cm with the evolution of magnetic active regions and with their ultraviolet and visible emissions is discussed by J. Donnelly *et al.* [*ibid.* **88**, 9883 (1983)].
8. The large-scale activity patterns responsible for the changes in global solar outputs of microwaves and the HeI 10830 and CaII radiations are discussed by V. Gaizauskas *et al.* [*Astrophys. J.* **265** (1983)].
9. G. Chapman and J. Boyden, *ibid.* **302**, L71 (1986).
10. D. Hoyt and J. Eddy, *Technical Note TN-194 + STR* (National Center for Atmospheric Research, Boulder, CO, 1982).
11. L. Oster *et al.*, *Astrophys. J.* **256**, 768 (1982).
12. J. Eddy, in *The Ancient Sun*, R. Pepin, J. Eddy, R. Merrill, Eds. (Pergamon, New York, 1980), p. 119.
13. Recent discussions of the sun's total irradiance variation estimated from photometry in visible light of spots and faculae have been presented by G. Chapman [*J. Geophys. Res.* **92**, 809 (1987)] and by J. Lawrence (*ibid.*, p. 813).
14. G. Chapman and T. McGuire, *Astrophys. J.* **217**, 657 (1977).
15. G. Brueckner *et al.*, *ibid.* **209**, 935 (1976).
16. J. Lean *et al.*, in *Solar Irradiance Variations on Active Region Time Scales*, B. Labonte *et al.*, Eds. (NASA conference publication 2310, Government Printing Office, Washington, DC, 1984). p. 253.
17. W. Lockwood and B. Skiff, unpublished results.

28 December 1987; accepted 30 March 1988

Protein Carbon-13 Spin Systems by a Single Two-Dimensional Nuclear Magnetic Resonance Experiment

BYUNG HA OH, WILLIAM M. WESTLER, PRASHANTH DARBA, JOHN L. MARKLEY*

By applying a two-dimensional double-quantum carbon-13 nuclear magnetic resonance experiment to a protein uniformly enriched to 26 percent carbon-13, networks of directly bonded carbon atoms were identified by virtue of their one-bond spin-spin couplings and were classified by amino acid type according to their particular single- and double-quantum chemical shift patterns. Spin systems of 75 of the 98 amino acid residues in a protein, oxidized *Anabaena* 7120 ferredoxin (molecular weight 11,000), were identified by this approach, which represents a key step in an improved methodology for assigning protein nuclear magnetic resonance spectra. Missing spin systems corresponded primarily to residues located adjacent to the paramagnetic iron-sulfur cluster.

RAPID PROGRESS HAS BEEN MADE in applying two-dimensional nuclear magnetic resonance (2D NMR) techniques (*1*) to proteins (*2*). Extensive ^{1}H NMR assignments have been obtained for more than 50 small proteins (*3*), and these assignments have enabled the determination of solution structures based on NMR cross-relaxation and coupling information (*2, 4*). Carbon-13 NMR has been neglected in the more popular strategies of protein spectroscopy, largely because of the low sensitivity of the experiment at the natural abundance concentration of ^{13}C (1.1%). Cross-assignments of ^{1}H-^{13}C groups in proteins have been achieved by 2D NMR approaches involving either ^{13}C detection (*5*) or the more efficient ^{1}H detection (*6*). However, extensive sequence-specific assignments are available to date only for the backbone carbon atoms of two small proteins (*7*), and only limited ^{13}C assignments of side chain resonances have been achieved (*8*).

In protein NMR spectroscopy, the conventional first step in obtaining sequence-specific assignments has been the analysis and classification of ^{1}H spin systems. This procedure requires the collection of 2D NMR data by two or more protocols [usually NOESY and COSY, as well as RELAY, HOHAHA, or similar methods (*9*)] followed by lengthy data-processing and spectral analysis. Some ambiguity usually exists in the spectral analysis because of similarities between the ^{1}H spin systems of several amino acid residues. For example, 8 of the 20 amino acids share the AMX spin system

Department of Biochemistry, College of Agricultural and Life Sciences, University of Wisconsin–Madison, 420 Henry Mall, Madison, WI 53706.

*To whom correspondence should be addressed.

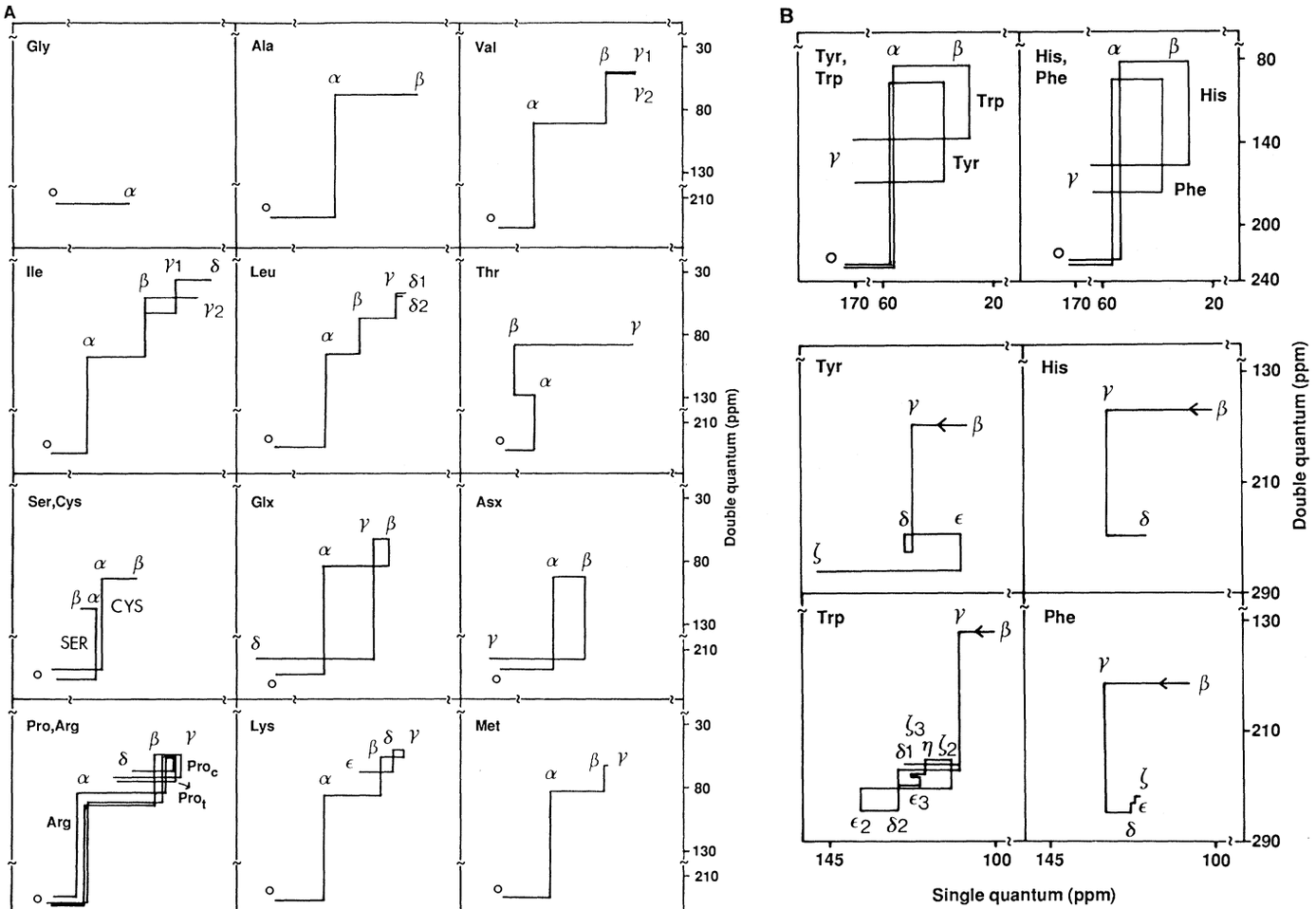

Fig. 1. Two-dimensional $^{13}C\{^{13}C\}DQC$ linkage patterns for the 20 common amino acid residues. This figure is based on ^{13}C NMR chemical shifts of the amino acids in small peptides (*25*): (**A**) aliphatic amino acids and (**B**) aromatic amino acids. Chemical shifts are referenced to $(CH_3)_4Si$.

(*2*). Only 8 to 15 of the 20 amino acid residue types (depending on the types of 2D ^1H NMR data sets collected) can be distinguished without recourse to sequence information. Although backbone resonances usually can be assigned, it is more difficult to obtain complete assignments of the longer chain amino acids such as lysine, proline, and those containing aromatic rings. These problems have hindered the complete assignment of side chain resonances in proteins.

An alternative approach to the analysis of protein NMR spectra is the determination of carbon-carbon connectivities by means of 2D homonuclear correlated spectroscopy ($^{13}C\{^{13}C\}$COSY) (*10*) or double-quantum correlated spectroscopy ($^{13}C\{^{13}C\}$DQC) (*10, 11*). The $^{13}C\{^{13}C\}$DQC (*12–15*) approach proved superior to $^{13}C\{^{13}C\}$COSY in a recent comparison involving a ^{13}C-labeled protein (*13*). In the $^{13}C\{^{13}C\}$DQC experiment, two directly bonded carbons A–B, whose ^{13}C peaks are located at δ_A and δ_B, give rise to cross peaks at $\delta_A/(\delta_A + \delta_B)$ and $\delta_B/(\delta_A + \delta_B)$. A survey of the expected linkage patterns is shown in Fig. 1. The only two amino acid pairs whose linkage patterns overlap are aspartate and asparagine (Asx) and glutamate and glutamine (Glx). Although the linkage patterns for arginine and proline are similar, they can be distinguished on the basis of their quite different Cδ chemical shift values. The wide range of ^{13}C chemical shifts (~190 ppm) compared with the much smaller environmental perturbations of these shifts (typically <4 ppm) facilitates the analysis. Carbon spin systems can be classified into 18 categories by a single $^{13}C\{^{13}C\}$DQC NMR experiment (Fig. 1).

With a molecule as large as a protein, the $^{13}C\{^{13}C\}$DQC approach requires ^{13}C isotopic enrichment. Signals are obtained only from pairs of directly bonded ^{13}C atoms. At the natural abundance of ^{13}C, the occurrence of such pairs is small (1.2×10^{-4}). Enrichment to a level of about 25% leads to an adequate signal-to-noise ratio while avoiding complications caused by passive coupling to nearby ^{13}C atoms (*13, 16*). Figure 2 shows the application of this approach to 26% uniformly labeled ^{13}C ($[U_{26\%}\ ^{13}C]$) ferredoxin from *Anabaena* 7120 (*17*). The high information content of the $^{13}C\{^{13}C\}$DQC map is perceived only upon expansion. For example, seven antiphase doublet peaks are resolved in the inset, which shows the threonine Cβ/(Cβ + Cγ) region. The $^{13}C\{^{13}C\}$DQC linkage pattern of one of these threonines is traced out in Fig. 2 [carbonyl carbon (C_0), 171.69 ppm; Cα, 60.74 ppm; Cβ, 67.76 ppm; and Cγ, 19.88 ppm) along with those of one isoleucine and one proline. Carbon-13 NMR chemical shifts of proline have been used to distinguish cis and trans X–Pro peptide bonds in small peptides (*18*). The proline whose spin system is outlined can be classified as trans by the positions of its Cγ/(Cβ + Cγ) and Cβ/(Cβ + Cγ) cross peaks (see Fig. 1). The $^{13}C\{^{13}C\}$DQC linkage pattern of the second resolved proline indicates that it also is trans. The ^{13}C spin systems of Asx and Glx were traced out by

starting from the Cβ/(Cβ + Cγ) or Cγ/(Cγ + Cδ) cross peaks of Asx and Glx, respectively, which lie in a region distinct from the Cα/(C_0 + Cα) cross peaks of the backbone carbonyls.

$^{13}C\{^{13}C\}$DQC spectra lend themselves to semiautomated graphic analysis. By using a graphics package developed for NMR analysis (*19*), the complete $^{13}C\{^{13}C\}$DQC spectrum was analyzed in about 1 week. Table 1 reports the numbers of complete ^{13}C spin systems identified. Discrepancies between the number of observed residues and the total based on the protein sequence appear to arise from hyperfine interactions between unpaired electrons of the 2Fe·2S* center and nearby carbon nuclei. $^{13}C\{^{13}C\}$DQC cross peaks will be absent whenever paramagnetic broadening leads to ^{13}C line widths that exceed the one-bond ^{13}C-^{13}C coupling constant (~30 to 70 Hz). In plant-type ferredoxins, the conserved amino acid residues of Ser^{40}, Gly^{44}, Ala^{43}, Ala^{45}, and Thr^{48} are reported to make hydrogen bonds to the 2Fe·2S* center (OH···S in the case of Ser^{40}, NH···S for the others) (*20, 21*). In addition, four cysteine residues are ligated directly to the 2Fe·2S* center (*20, 21*). Thus one expects resonances from 2 Ala, 4 Cys, 1 Gly, 1 Ser, and 1 Thr to be missing. The results in Table 1 agree with this prediction. At least some of the 14 other missing ^{13}C spin systems (1 Arg, 3 Asx, 4 Glx, 3 Leu, 1 Lys, 1 Pro, and 1 Val) probably represent additional amino acid residues within about 10 Å of the 2Fe·2S* center.

Cross-assignment of directly bonded ^1H-^{13}C pairs by means of a $^1H\{^{13}C\}$ heteronuclear multiple-quantum experiment (*6*) serves to identify the proton spin systems. The combination of $^{13}C\{^{13}C\}$DQC and $^1H\{^{13}C\}$ experiments offers an efficient approach to analyzing protein NMR spectra that has distinct advantages over the methods in current use (described above). A striking feature of the $^{13}C\{^{13}C\}$DQC map (Fig. 2) is its simplicity; it contains well-resolved regions for all 18 amino acid types. With a diamagnetic protein, the results, when combined with sequence-specific resonance assignment techniques (*2, 13*), will support analysis of amino acid sequences as well as amino acid compositions. The results will also enable the detection of posttranslational modification of amino acid residues and the detection and assignment of spin systems of carbon-containing prosthetic groups (*16*). The only ambiguities found for the 20 common amino acids, Glu = Gln and Asp = Asn, can be resolved readily by dual ^{13}C-^{15}N labeling (*22*). Modern methods of biotechnology support the efficient production of labeled proteins at moderate cost (*23*). For proteins that can be overproduced, the ease of analysis of $^{13}C\{^{13}C\}$DQC spectra justifies the added expense of the stable isotope.

The facile analysis of ^{13}C spin systems should greatly simplify sequence-specific assignments based on dual ^{13}C-^{15}N labeling (*24*). Previously, the assignment of each unique dipeptide by this method has required the introduction of $^{13}C_0$ into one amino acid residue type along with the introduction of $^{15}N\alpha$ into the same or another residue type (*24*). Since the $^{13}C_0$ resonances can be classified by the $^{13}C\{^{13}C\}$DQC experiment, it should be sufficient to use uniform ^{13}C labeling (~25%) along with specific ^{15}N labeling of individual amino acids. Implementation of a 2D ^{13}C-^{15}N correlation experiment would permit sequence-specific assignments to be achieved with a single protein sample uniformly labeled with both ^{13}C and ^{15}N (*22*).

Assignments of ^{13}C resonances are useful in their own right. They are needed, for example, in dynamics studies based on ^{13}C relaxation and in determinations of the pK_a values of ionizable groups based on the *p*H dependence of carbon chemical shifts. In addition to greatly facilitating the assignment of ^{13}C spectra, we expect that the $^{13}C\{^{13}C\}$DQC approach will find use in the assignment of ^1H and ^{15}N signals in protein NMR spectra.

Table 1. Number of amino acid residues of oxidized *Anabaena* 7120 ferredoxin identified by their two-dimensional $^{13}C\{^{13}C\}$DQC linkage pattern compared with the amino acid composition of the protein (in parentheses). The amino acid composition is based on the sequence of the protein (*21*).

Ala 7 (9)	His 2 (2)	Pro 2 (3)
Arg 0 (1)	Ile 5 (5)	Ser 5 (6)
Asx 9 (12)	Leu 4 (7)	Thr 7 (8)
Cys 0 (4)	Lys 3 (4)	Trp 0 (0)
Glx 11 (15)	Met 0 (0)	Tyr 5 (5)
Gly 5 (6)	Phe 3 (3)	Val 7 (8)

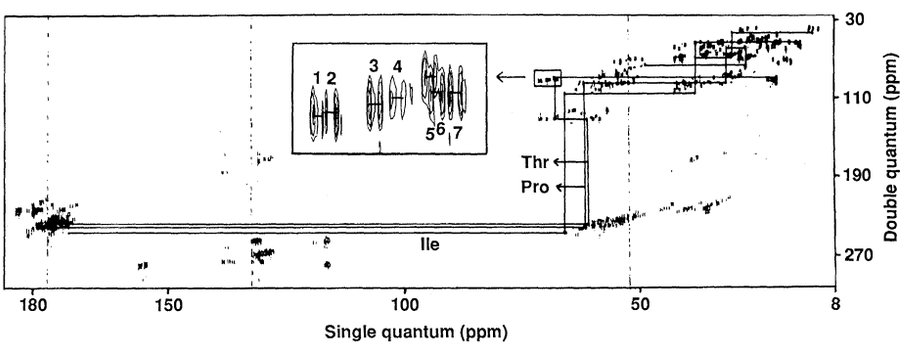

Fig. 2. Two-dimensional $^{13}C\{^{13}C\}$DQC spectrum obtained with oxidized [$U_{26\%}$ ^{13}C]ferredoxin from *Anabaena* 7120. The inset shows a blowup of the threonine Cβ/(Cβ + Cγ) region. $^{13}C\{^{13}C\}$DQC linkage patterns are outlined for one Thr, one Ile, and one Pro residue. Chemical shifts are referenced to $(CH_3)_4Si$.

REFERENCES AND NOTES

1. A. Bax and L. Lerner, *Science* **232**, 960 (1986); R. R. Ernst, G. Bodenhausen, A. Wokaun, *Principles of Nuclear Magnetic Resonance in One and Two Dimensions* (Clarendon, Oxford, 1987).
2. K. Wüthrich, *NMR of Proteins and Nucleic Acids* (Wiley-Interscience, New York, 1986).
3. Tabulated in J. L. Markley, E. L. Ulrich, Y. Kyogoku, *Protein Sequences Data Anal.*, in press.
4. G. M. Clore and A. M. Gronenborn, *Protein Eng.* **1**, 275 (1987).
5. W. M. Westler, G. Ortiz-Polo, J. L. Markley, *J. Magn. Reson.* **58**, 354 (1984); T.-M. Chan and J. L. Markley, *J. Am. Chem. Soc.* **104**, 4010 (1982).
6. For a review, see R. H. Griffey and A. G. Redfield, *Q. Rev. Biophys.* **19**, 51 (1987).
7. G. Wagner and D. Brühwiler, *Biochemistry* **25**, 5839 (1986); A. D. Robertson, G. I. Rhyu, W. M. Westler, J. L. Markley, unpublished results.
8. Tabulated in J. L. Markley and E. L. Ulrich, *Annu. Rev. Biophys. Bioeng.* **13**, 493 (1984).
9. NOESY, nuclear Overhauser effect spectroscopy [A. Kumar, R. R. Ernst, K. Wüthrich, *Biochem. Biophys. Res. Commun.* **95**, 1 (1980)]; COSY, correlated spectroscopy [K. Nagayama, A. Kumar, K. Wüthrich, R. R. Ernst, *J. Magn. Reson.* **40**, 321 (1980)]; RELAY, relayed correlated spectroscopy [A. Bax and G. Drobny, *ibid.* **61**, 306 (1985)]; HOHAHA, homonuclear Hartmann-Hahn spectroscopy [D. G. Davis and A. Bax, *J. Am. Chem. Soc.* **107**, 2820 (1985)].
10. J. L. Markley, W. M. Westler, T.-M. Chan, C. L. Kojiro, E. L. Ulrich, *Fed. Proc.* **43**, 2648 (1984).
11. A. Bax, R. Freeman, S. P. Kempsell, *J. Am. Chem. Soc.* **102**, 4849 (1980).
12. The pulse sequence used (*13*) is that of Levitt and Ernst (*14*), except that time-proportional phase increments [TPPI (*15*)] with 45°-phase increments has been added to the double-quantum propagator to achieve pure-phase 2D spectra and quadrature detection in ω_1. The name INADEQUATE (incredible natural abundance double-quantum transfer experiment) was applied originally (*11*) to a simpler pulse sequence; it implies that the data are acquired at natural abundance ^{13}C. We have adopted the name "carbon-carbon double-quantum correlation" or "$^{13}C\{^{13}C\}$DQC" spectroscopy (*13*) for the method described here.
13. W. M. Westler, M. Kainosho, H. Nagao, N. Tomonaga, J. L. Markley, *J. Am. Chem. Soc.*, in press.
14. M. L. Levitt and R. R. Ernst, *Mol. Phys.* **50**, 1109 (1983).
15. G. Drobny, A. Pines, S. Sinton, D. Weitekamp, D. Wemmer, *Faraday Div. Chem. Soc. Symp.* **13**, 49 (1979); G. Bodenhausen, R. L. Vold, R. R. Vold, *J. Magn. Reson.* **37**, 93 (1980).
16. B. J. Stockman, W. M. Westler, P. Darba, J. L. Markley, *J. Am. Chem. Soc.*, in press.
17. We obtained [$U_{26\%}$ ^{13}C]ferredoxin by growing *Anabaena* 7120 (a cyanobacterium) on [$U_{26\%}$ ^{13}C]CO_2. The sample used for acquiring the NMR spectrum was 9 m*M* oxidized [$U_{26\%}$ ^{13}C]ferredoxin in 0.5 ml of ^2H_2O containing 25 m*M* phosphate

buffer, uncorrected *p*H meter reading 6.1; 220 blocks of free induction decays were collected as 8192 data points (each represented the average of 800 transients). The recycling time for each accumulation was 1.16 seconds, and the total experiment time was 74 hours. The level of enrichment was determined by measuring the ^{13}C satellite peaks in the ^{1}H NMR spectrum of proline isolated from a protein hydrolyzate.
18. C. Grathwohl and K. Wüthrich, *Biopolymers* **15**, 2025 (1976).
19. The software package used was "MADNMR," an interactive graphics program written for the Silicon Graphics IRIS 2400 workstation (P. Darba and J. L. Markley, unpublished results).
20. T. Tsukihara, K. Fukuyama, Y. Katsube, in *Iron-Sulfur Protein Research*, H. Matsubara, Y. Katsube, K. Wada, Eds. (Japan Scientific Society Press, Tokyo, 1986), pp. 59–68; the numbering system used here is that used in (*21*).
21. J. Alam, R. A. Whitaker, D. W. Krogmann, S. E. Curtis, *J. Bacteriol.* **168**, 1265 (1986).
22. Preliminary $^{13}C\{^{15}N\}$ heteronuclear chemical shift correlation studies involving [$U_{26\%}$ ^{13}C, $U_{95\%}$ ^{15}N]flavodoxin and [$U_{26\%}$ ^{13}C, $U_{95\%}$ ^{15}N] ferredoxin indicate the feasibility of this approach; W. M. Westler, B. J. Stockman, B. H. Oh, J. L. Markley, unpublished results.
23. J. L. Markley, in *Protein Engineering*, D. Oxender and C. F. Fox, Eds. (Liss, New York, 1987), pp. 15–33.
24. M. Kainosho and T. Tsuji, *Biochemistry* **21**, 6273 (1982).
25. R. Richarz and K. Wüthrich, *Biopolymers* **17**, 2133 (1978).
26. We thank D. A. Benway, B. J. Stockman, and E. S. Mooberry for their assistance. Supported by USDA competitive grant 85-CRCR-1-1589 and National Institutes of Health grant RR02301 from the Biomedical Research Technology Program, Division of Research Resources. This study made use of the National Magnetic Resonance Facility at Madison, which is supported in part by grant RR02301. Additional equipment in the facility was purchased with funds from the University of Wisconsin, the NSF Biological Biomedical Research Technology Program (grant DMB-8415048), NIH Shared Instrumentation Program (grant RR02781), and the U.S. Department of Agriculture.
8 February 1988; accepted 5 April 1988

Calpain II Involvement in Mitosis

JUDITH E. SCHOLLMEYER

Mitotic spindle disassembly requires major structural alterations in the associated cytoskeletal proteins and mitosis is known to be associated with Ca^{2+}-sequestering phenomena and calcium transients. To examine the possible involvement of a ubiquitous Ca^{2+}-activated protease, calpain II, in the mitotic process, synchronized PtK_1 cells were monitored by immunofluorescence for the relocation of calpain II. The plasma membrane was the predominant location of calpain II in interphase. However, as mitosis progressed, calpain II relocated to (i) an association with mitotic chromosomes, (ii) a perinuclear location in anaphase, and (iii) a mid-body location in telophase. Microinjection of calpain II near the nucleus of a PtK_1 cell promoted the onset of metaphase. Injection of calpain II at late metaphase promoted a precocious disassembly of the mitotic spindle and the onset of anaphase. These data suggest that calpain II is involved in mitosis.

THE REDISTRIBUTION OF Ca^{2+} (*1–4*) and calcium-binding proteins (*5*, *6*) during the mitotic cycle has been well documented. Additionally, disassembly of the mitotic spindle (*7*, *8*) or microtubules in lysed cells (*9*) has been shown to be Ca^{2+}-dependent. In this study, I have examined the possibility that a Ca^{2+}-activated protease, calpain II (E.C. 3.4.22.17), may be involved directly or indirectly in the mediation of specific mitotic events by Ca^{2+}. In the first part of the study PtK_1 cells were synchronized by a double thymidine block and then monitored via immunofluorescence for the redistribution or translocation of calpain II (Fig. 1). At plating of the cells (prometaphase), calpain II appeared to be exclusively associated with the chromosomes (Fig. 1a). As mitosis proceeded, calpain II remained associated with the chromosomes during early and late anaphase (Fig. 1, b and c) but then was observed at a bilaterally symmetrical location at the periphery of the cells as well as in association with the cytoplasmic bridge during telophase or cytokinesis (Fig. 1d). An example of one daughter cell at the end of cytokinesis is shown with remaining mid-body (Fig. 1e). Finally, at interphase, calpain II had a predominantly plasma membrane association (Fig. 1f). Different stages of mitosis shown in Fig. 1 are representative of approximately 20 cells for each panel.

In order to better assess the dynamic nature of the calpain II involvement in mitosis, microinjection techniques were used to place rhodamine isothiocyanate–labeled calpain II (calpain II–RITC) at selected cellular locations and then monitor calpain II translocation and the time required for the completion of mitotic stages.

Calpain II–RITC injected near the nucleus of a cell in interphase (Fig. 2, a and b) promoted the onset of metaphase, and the labeled calpain II quickly became associated with the metaphase chromosomes (Fig. 2c). Onset of metaphase occurred approximately 5 minutes after calpain II–RITC injection at interphase. The same cells, shown as they progressed through anaphase displayed redistribution of calpain II–RITC from a predominantly chromosomal association (Fig. 2d) to a bilaterally symmetrical location near the reforming nucleus and association with the cytoplasmic bridge (Fig. 2, e and f). One daughter cell, shown 1 hour after calpain II–RITC injection, displayed calpain II–RITC staining associated exclusively with the plasma membrane (Fig. 2g). Cells injected at late metaphase display a more rapid than normal transition from metaphase to anaphase (approximately 1 to 1.5 minutes relative to a normal transition time for PtK cells of 16 minutes) and the injected calpain II–RITC appeared to condense at the middle of the cytoplasmic bridge (Fig. 2i), with eventual localization at the mid-body of daughter cells (Fig. 2j). Although the fluorescence pattern seen in Fig. 2j is not identical with that in Fig. 2, e and f, or Fig. 1c, this is a staining pattern frequently seen in cells that have been neither injected nor synchronized. Results obtained after microinjection of unlabeled calpain II paralleled those seen with calpain II–RITC. Control injections of similar volumes and protein loads of bovine serum albumin–conjugated RITC (BSA-RITC) did not appear to promote metaphase or anaphase.

Microinjection techniques were then used to examine the Ca^{2+} requirements of calpain

Table 1. Effect of interaction of Ca^{2+}, calpain II, and calpastatin on anaphase onset. Injection was made in synchronized cells shortly after plating; by inspection these cells were seen to be in metaphase. Twenty cells were injected for each treatment.

[Ca^{2+}] (μM)	Calpain II (1 mg/ml)	Calpastatin* (1 mg/ml)	Onset of anaphase, time in minutes ($\bar{X}$ ± SE)
0.1	−	−	14 ± 1.3
1.0	−	−	3 ± 0.9
5.0	−	−	5 ± 1.3
10.0	−	−	15 ± 1.5
0.1	+	−	2 ± 0.5
1.0	+	−	3 ± 0.6
5.0	+	−	3 ± 0.7
10.0	+	−	11 ± 0.8
0.1	−	+	15 ± 1.7
1.0	+	+	†
5.0	+	+	†
10.0	−	+	17 ± 1.2
Buffer alone	−	−	14 ± 1.8

*Homogenous preparation of calpastatin (170 kD) from porcine skeletal muscle was used in these studies. Purification and biochemical characterization of porcine skeletal calpastatin has been described (*30*). †Cells did not progress to anaphase.

U.S. Department of Agriculture, Agricultural Research Service, Roman L. Hruska Meat Animal Research Center, Clay Center, NE 68933.